FULL PAPER

Selective Alignment of Molecular Glass Wrinkles by Engineered Magnetic Field Landscapes

Henning Huckfeldt, Florian Ahrend, Dennis Holzinger, Holger Klein, Dieter Engel, Michael Melzer, Denys Makarov, Oliver G. Schmidt, Thomas Fuhrmann-Lieker, and Arno Ehresmann*

A new approach for aligning wrinkles in thin viscoelastic polymethylmethacrylate films is established by sandwiching them between ferromagnetic layers. Experiments prove that a contribution from an engineered anisotropic 1D periodic magnetic stray field pattern can be decisive for the alignment of otherwise randomly oriented wrinkles at commensurate periods of the magnetic template pattern and the wrinkles. Alternatively, random wrinkling is observed under similar conditions, but when periodic magnetic stray fields are missing or not commensurate with the wrinkle wavelength. The possibility to stabilize two distinct types of wrinkling patterns in the same material system paves the way toward mechanically reconfigurable functional elements, enabling exciting possibilities for stretchable electronics, magnetic field sensors, and tuneable gratings for optoelectronics and photonics.

1. Introduction

Bottom-up self-organization of nanoscale objects or molecules enables the realization of versatile metastructures spreading from self-assembling nanoparticles, metal-organic frameworks up to DNA-origami.[1–3] One prominent example is the so called "wrinkling" (or "buckling") phenomenon, which usually occurs when a strained heterostructure of a viscoelastic layer capped with a rigid thin film is heated above its glass transition temperature and is subsequently cooled down.[4,5] As a result of the wrinkling a wavy surface of the viscoelastic layer is obtained (**Figure 1**) which, however, does not lead to a delamination from the substrate. In the case of isotropic boundary conditions, no preferred orientation of the wrinkling process is observed which, in general, leads to a labyrinth-like structure (Figure 1a) on a larger scale, but particular material systems or sample treatments can lead to a number of different morphologies.[6–8]

While wrinkles can be of vital use to gain access to mechanical properties of thin films,[9–11] the excess of surface area of the wrinkles in comparison to their 2D projection additionally allows for a widespread application in stretchable electronics[12–14] including interconnects[15,16] and functional elements, e.g., temperature[17] or magnetic field sensors[18–20] and even integrated circuits.[21] Beyond these applications, aligned wrinkles (Figure 1b,c) are of great relevance for the realization of periodic templates, e.g., gratings[22] or distributed feedback laser components.[23] Typically, an alignment of wrinkles is achieved either by the induction of directed stress during fabrication using flexible substrates[8,9,24] or by the use of topographic elevations in patterned substrates.[5,7,25,26] Whereas the latter method results in discontinuities of the wrinkle pattern, the first one necessitates flexible substrates which can be a disadvantage for device integration. Therefore, a method is lacking to produce aligned wrinkles over large areas without interceptions in the wrinkling periodicity on a rigid support as required for integration purposes to apply the full spectrum of conventional microelectronic and thin film fabrication techniques. Furthermore, the control of the wrinkling process, i.e., the deliberate choice between random and aligned wrinkling, would pave the way toward the realization of reconfigurable wrinkling templates and allow for completely new possibilities in research and device development.

H. Huckfeldt, F. Ahrend, D. Holzinger, H. Klein, Prof. A. Ehresmann
Department of Physics and Center for Interdisciplinary Nanostructure Science and Technology (CINSaT)
Kassel University
Heinrich-Plett-Strasse 40, 34132 Kassel, Germany
E-mail: huckfeldt@physik.uni-kassel.de
Dr. D. Engel
Helmholtz-Zentrum Berlin für Materialien und Energie
Research Group Functional Nanomaterials
Hahn-Meitner-Platz 1, 14109 Berlin, Germany
M. Melzer, Dr. D. Makarov, Prof. O. G. Schmidt
Leibniz Institute for Solid State and Materials Research Dresden (IFW Dresden)
Institute for Integrative Nanosciences
Helmholtzstrasse 20, 01069 Dresden, Germany
Prof. T. Fuhrmann-Lieker
Department of Chemistry and Center for Interdisciplinary Nanostructure Science and Technology (CINSaT)
Kassel University
Heinrich-Plett-Strasse 40, 34132 Kassel, Germany

DOI: 10.1002/adfm.201503155

2. Results

Here, we demonstrate a new approach for aligning wrinkles in thin viscoelastic polymethylmethacrylate (PMMA) films. The approach for aligned wrinkling is based on the fine tuning of

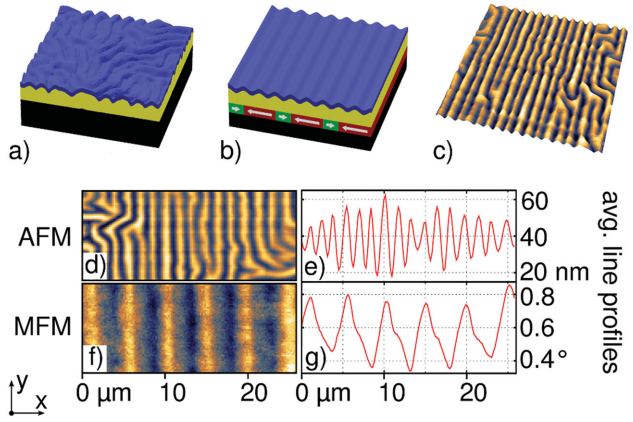

Figure 1. Schematic images of the layer system and topography of a) a randomly wrinkled film consisting of a rigid substrate, a viscoelastic layer, and a thin film cap, where surface deformations, induced by material strain, occur. b) A material system for magnetically induced aligned wrinkling with intermediate exchange bias layers magnetically patterned by light ion bombardment. Magnetostatic interactions from stray fields with a ferromagnetic capping layer influence the wrinkling. c) 3D image of the surface of a magnetically aligned wrinkled surface measured by AFM. In d) exemplary AFM data with aligned wrinkles are shown, with the corresponding averaged horizontal line profile in e). The corresponding MFM signal of the same area, showing the stray field gradient originating from Néel type domain walls in the magnetically patterned exchange bias system, is depicted in f) with its horizontal line profile in g). By comparing d) with f) or e) with g), the fixed phase relation between wrinkles and magnetic signal becomes obvious.

the mechanical energy of the material system during the formation of wrinkles by means of magnetic stray fields. Our experiments show that a small impact from magnetostatic interaction between two magnetic thin films (energy scale of a few hundred meV nm^{-2}, see Note S1, Supporting Information) can dramatically influence the mechanical energy landscape of the viscoelastic system (energy scale of about 100 eV nm^{-2},[27] see Note S2, Supporting Information). It turns out that the contribution of an engineered anisotropic 1D periodic magnetic stray field pattern is crucial for the alignment of otherwise randomly oriented wrinkles, when the periodicity of both the magnetic template and the wrinkles is commensurate while heating the sample. Since the wrinkling process is mediated by the stray fields emanating from specifically designed magnetic domain wall structures of a magnetically stripe patterned substrate, the wrinkles are found to align along the magnetic domain walls during the nucleation process, which results in a 1D periodic template at the large scale (compare Figure 1d,e and Figure 1f,g showing the morphology of the wrinkles and the underlying magnetic domain pattern, respectively). By contrast, random wrinkling is observed under identical conditions if periodic magnetic stray fields are missing or are not commensurable with the wrinkle wavelength.

To align wrinkles over a macroscopic area, a PMMA layer is sandwiched between two ferromagnetic thin films. We engineered a spatially periodic landscape of magnetic stray fields with stripe structure by modifying the magnetic properties of the bottom ferromagnetic layer, consisting of CoFe (6.5 nm) exchange-bias (EB) coupled to a 10 nm thick IrMn layer, using ion bombardment induced magnetic patterning (IBMP).[28–31] This process does not result in topographic modifications of the sample surface.[28] For the experiments shown here, magnetic parallel stripe domains of alternating widths W_s = (1.45 ± 0.05) µm and W_l = (2.55 ± 0.05) µm and lengths over several millimeters were patterned (Figure 1f,g). Stripes of alternating widths were prepared to differentiate between domains where the magnetization is pointing in $+x$ or $-x$ direction using magnetic force microscopy.

As the magnetic moments of neighboring stripes are oppositely in-plane oriented toward the long edge of the stripes and the domains are separated by Néel type domain walls, stray fields emanate at the boundaries between neighboring domains.[32,33] The thickness of 6.5 nm of the bottom ferromagnetic layer was chosen as a compromise between maximum stray fields (which scale with the layer thickness) and a fully shifted magnetic hysteresis loop for the remnant artificial domains, which is needed to achieve a well-defined magnetic stray field landscape (see the Experimental Section for further details).[30,34] A 9 nm thick CoFe layer on top of the PMMA is used as upper ferromagnetic film in this study. Due to the grainy morphology of the polycrystalline CoFe film grown by sputter deposition on top of the PMMA layer, a modification of the thickness of the top ferromagnetic layer does not influence the resulting mechanical strain before wrinkling formation and, therefore, does not qualitatively change the results presented in this work.

To initialize wrinkling, the samples were annealed on a hotplate, where they were heated up to 150 °C for 1 min (Experimental Section). The strongest impact of the stray field landscape produced by the parallel stripe domains on the wrinkling is found when the period of the wrinkles is commensurate to the width of the magnetic domains (**Figures** 1g and **2**a). Random wrinkling is observed if the patterns are not commensurate (Figure 2b) or if there is no pattern at all (Figure 2c).

To correlate the structure of the magnetic pattern with the wrinkle wavelength, we relied on the well-established feature that the thickness of the viscoelastic layer determines the period and amplitude of the wrinkles.[35] In our case, for a (92 ± 3) nm thick PMMA layer, an average peak-to-peak amplitude of $2A$ = (80 ± 15) nm was observed, obtained as the full width at half maximum (FWHM) of the height distribution of the atomic force microscope (AFM) measurements. The corresponding wrinkling wavelength was W_w = (1.33 ± 0.10) µm. With this wavelength, the best alignment of wrinkles was observed as the patterns are very close to commensurability: in the case of smaller magnetic domains the ratio of W_s/W_w = 1.1 ≈ 1 is achieved, while for the wider magnetic domains we obtain W_l/W_w = 1.9 ≈ 2. This is revealed by the analysis of atomic and magnetic force microscope (AFM/MFM) images which show a fixed relation in period and phase between the wrinkles and the magnetic pattern of the substrate. This relation leads to the location of a topographic maximum above each magnetic domain wall and in the center of each wider magnetic domain (compare Figure 1d,f and Figure 1e,g). The parallel alignment of the wrinkles extends over areas of at least 20 × 20 µm^2 (Figure 2a). The topographic maxima of the wrinkles are located over the domain walls with a variance of less than 15% of the wrinkling wavelength as observed for several areas on multiple samples.

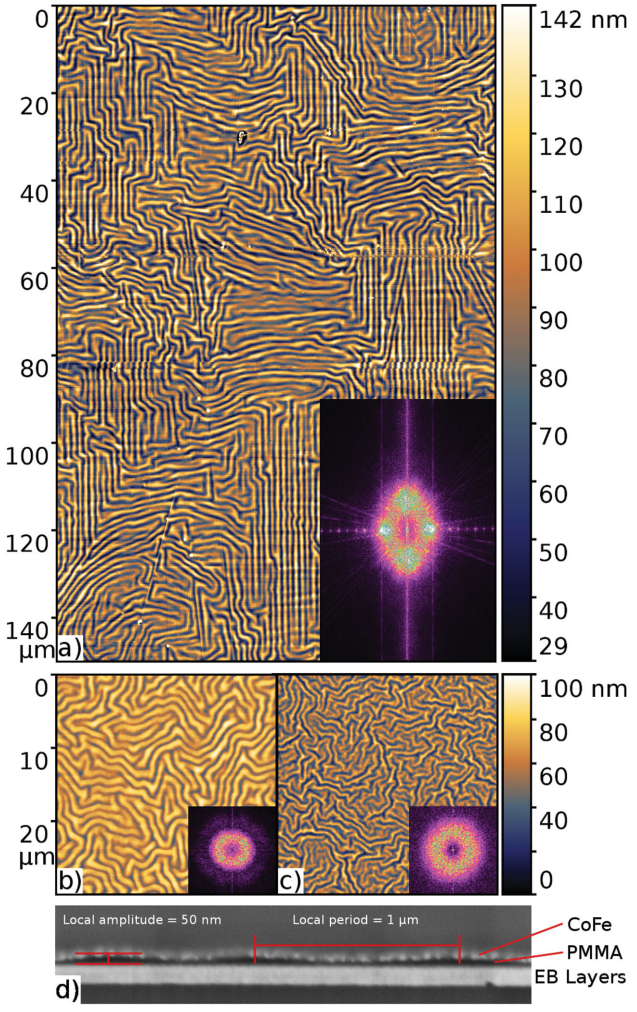

Figure 2. AFM data from wrinkled surfaces under different scenarios. The insets show the corresponding FFT of the surface data. a) Wrinkling on top of a magnetically patterned EB system under commensurate conditions. The magnetic domain walls are oriented vertically. Areas of wrinkles aligned to the domain walls are visible intermitted from areas with perpendicular orientation. This is also indicated in the FFT, which shows slightly different wavelengths for parallel and perpendicularly aligned wrinkles. In addition, equidistant horizontal spots in the FFT indicate the highly periodic structure of the surface. In b) and c) randomly oriented wrinkles on top of EB systems are shown where a noncommensurate magnetic pattern and, respectively, no pattern at all has been applied. The circular FFT data reveal the arbitrary orientation of the wrinkles. d) SEM cross-section image of the wrinkled layer system fabricated by focused ion beam etching. Individual layers are well separated and the thickness variation of the PMMA layer is clearly visible. The fluctuating intensity of the topmost CoFe layer originates from its grain structure.

3. Discussion

The in-depth analysis of the topographic AFM data is further performed using 2D fast Fourier transformation (2D-FFT). The 2D-FFT in Figure 2a features periodic spots which can be tracked back in the real space to the presence of a long range order of the wrinkling pattern parallel to the *x*-axis with a periodicity of 1.33 µm. We attribute the appearance of the 1D arrangement of wrinkles, which are aligned with respect to the underlying magnetic domain pattern, to the impact of the magnetic stray fields on the mechanical energy of the system during the formation of wrinkles, as will be discussed below. Interestingly, in addition to the wrinkles oriented parallel to the magnetic domain pattern, comparable areas with wrinkles oriented mainly perpendicular to the magnetic field landscape, i.e., along the *y*-axis are observed. An analysis of the 2D-FFT image allows an estimation of the periodicity of this pattern which is equal to $W = 1.72$ µm. An explanation for the appearance of the two orthogonally oriented areas of aligned wrinkles requires the understanding of the wrinkling process in metal-capped PMMA layers.

For the wrinkling mechanism, the source of the lateral stresses between metal and polymer films has to be identified. In the investigated samples, the stress is already induced during the deposition of the CoFe top layer. This assumption was cross-checked by growing a similar 9 nm thick CoFe film onto a smooth elastomeric polydimethylsiloxane (PDMS, Dow Corning Sylgard 184 10:1) membrane using identical deposition parameters. Due to the lower Young's modulus of PDMS compared to PMMA, the top surface of this reference sample wrinkles immediately after preparation (Figure S3, Supporting Information). The lateral strain in the ferromagnetic CoFe film prepared on PMMA is quantified from the AFM data (calculated from the difference in total surface area to the total area scanned) resulting in 0.75% areal compression. However, keeping in mind that the Young's modulus of PMMA at room temperature is about 2 GPa, the accumulated stress in the metal films is insufficient to induce wrinkles while depositing the metal film at room temperature.

We propose that the wrinkles are formed during the annealing of the sample, which has strong impact on the mechanical parameters of the polymeric PMMA layer. Indeed, while annealing up to 150 °C, the PMMA exceeds the glass transition temperature (114 °C),[36] which can substantially lower the Young's modulus of the polymer. To check this assumption, we carried out in situ laser scattering experiments (**Figure 3**a) that allow us to follow the transformation of the topography of the sample from the practically flat one to the wrinkled system during annealing. The measurement reveals that a strong enhancement of the scattering intensity is first detected when the sample temperature rises above 90 °C (Figure 3b). This feature is correlated with the formation of wrinkles. The fact that the wrinkles occur during heating indicates that there is substantial stress already present in the sample, which also supports the assumption of deposition induced stress. The observed modification of the wrinkle period during heating indicates the softening of the PMMA layer. We applied the empiric approach of Bowden et al.[7] to assess Young's modulus of the PMMA at different temperatures by monitoring the wrinkle period: in the case of $W_w = 0.9$ µm (at $T = 95$ °C) a Young's modulus of 14.4 MPa is estimated. An increase of the wrinkling period to 2.1 µm (at $T = 160$ °C) results in the Young's modulus of 1.1 MPa, which is a typical value for a soft elastomer, e.g., PDMS.[18] Please note that the theory[7] is perfectly applicable in this case as there is a tight binding between metal and polymer. The latter is evidenced by cross-sectional analysis of the sample morphology (Figure 2d) imaged using

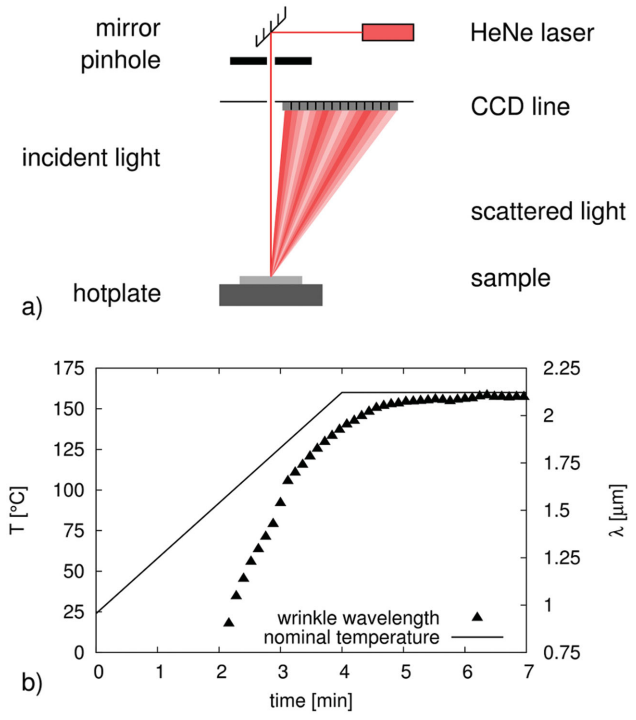

Figure 3. a) Set-up for in situ surface light scattering experiments and b) the gathered data. The scattered light intensity on the CCD line sensor is directly correlated to the wrinkle period. The initial detection of wrinkles while heating with a constant rate was possible after about 2 min at a nominal temperature of 90 °C and continuously increased toward a final wavelength of about 2.1 µm at 160 °C.

scanning electron microscopy (SEM). The cross-section was prepared using focused ion beam (FIB) etching.

While the sample is cooling down to room temperature, the period shrinks again and finally reaches the experimentally observed value of about 1.33 µm. At this point, the PMMA restores its hardness (2 GPa) revealing the aligned wrinkles, which are frozen in the PMMA.

There are two possible models that have to be considered when the alignment of wrinkles in the initially in-plane isotropic system could take place. The first one assumes that the wrinkle alignment takes place already at the nucleation point of $T = 90$ °C. This spontaneous alignment could be initiated by the anisotropic relaxation of the isotropic mechanical stress in the system, which is dictated by the anisotropic contribution from the magnetic interaction. In this model, the wrinkles are aligned from the very beginning of their appearance and only the periodicity but not the symmetry of this so formed anisotropic wrinkling pattern is affected by the further annealing treatment. For this mechanism, the magnetic energy landscape should have peculiarities (e.g., extrema) of the stray field gradient resulting in the force to the top CoFe film at the locations covering the range of x-coordinates from 0.9 to 2.1 µm. This requires that extrema of the energy landscape should be rather broad.

The second model assumes that the isotropic wrinkling pattern nucleates with the period of 0.9 µm at $T = 90$ °C. During further annealing, when the period reaches about 1.3 µm (at $T = 110$ °C), alignment of wrinkles takes place, because the pattern is commensurate to the underlying magnetic template at this point. In this case, the magnetic energy landscape should have rather narrow extrema clearly defining the bending points at the surface of the top CoFe layer at the locations of the magnetic domain walls and in between the broad domain (three periods of the topographic pattern correspond to one period of the magnetic template). The magnetic stray field profile has to be considered in order to assess which of these two models is valid for our system.

Spatially resolved micro-Hall measurements between 750 and 2650 nm above the substrate surface were extrapolated to assess the out-of-plane component of the magnetic field of $H_z \approx 2.5$ kA m^{-1} at a distance of about 100 nm above the sample.[33] This value was used to calibrate the amplitude of the numerical simulations, which assume an arctan transition of the magnetization vector between adjacent magnetic domains. The magnetic stray fields can be than calculated by using an analytical expression.[33] These calculations show the decay of the magnetic stray fields in x- and z-directions emerging from the domain walls of the patterned substrate as depicted in **Figure 4**d. It is obvious that these stray fields are much smaller than the saturation field in the out-of-plane direction (≈200 kA m^{-1}, **Figure 5**d) of the upper CoFe layer and are therefore not sufficient to tilt the in-plane magnetization of the top CoFe film, even at locations directly above the Néel domain walls. Keeping in mind that, in the case of the stripe domain pattern with a Néel type domain wall structure, the y-component of the magnetic field is constant and independent of the coordinate, the only relevant component of the magnetic stray field is H_x. The performed numerical calculations allow us to assess the variation of H_x along the x-axis as shown in Figure 4d.[32,33] As expected, H_x exhibits a zero-crossing directly above each domain wall and increases heavily near to it. The highest value of H_x is achieved at around 250 nm from the domain wall. In the center of each domain the absolute value of the stray field component exhibits a local minimum. From this data the gradient of H_x along the x-axis can be derived which exhibits three minima and three maxima of different amplitudes along one period of the magnetic pattern (Figure 4c). These correlate in number to the topographic extrema of the wrinkles (Figure 4b). The minima and maxima in the stray field gradient do not share the exact same location as those of the wrinkles, as the extrema of the stray field gradient are not equally distributed (Figure 4c). An exact replication by the wrinkles would be energetically unfavorable in terms of the bending energy of the capping layer and therefore does not take place. In contrast, wrinkle extrema are located directly above each domain wall while there is a single wrinkle period over each small magnetic domain and two periods above each wider magnetic domain (Figure 4a,b). As stated above, this asymmetry in the wrinkle pattern with respect to the magnetic stray fields originates from the pattern of magnetic domains with unequal widths.

From the strength of the magnetic field gradient, $\partial H_x/\partial x = 1000$ kA m^{-2}, and the saturation magnetization ($M_S = 1800$ kA m^{-1})[32] of the CoFe alloy, the in-plane force per unit area of about 20 mN m^{-2} is estimated (see Note S1, Supporting Information). This force acts on the top CoFe layer along the x-axis trying to deform the magnetic layer predominantly at the locations of the extrema of the stray field gradient and is the magnetic energy contribution to the mechanical energy of the system consisting of the inherent strain and the bending

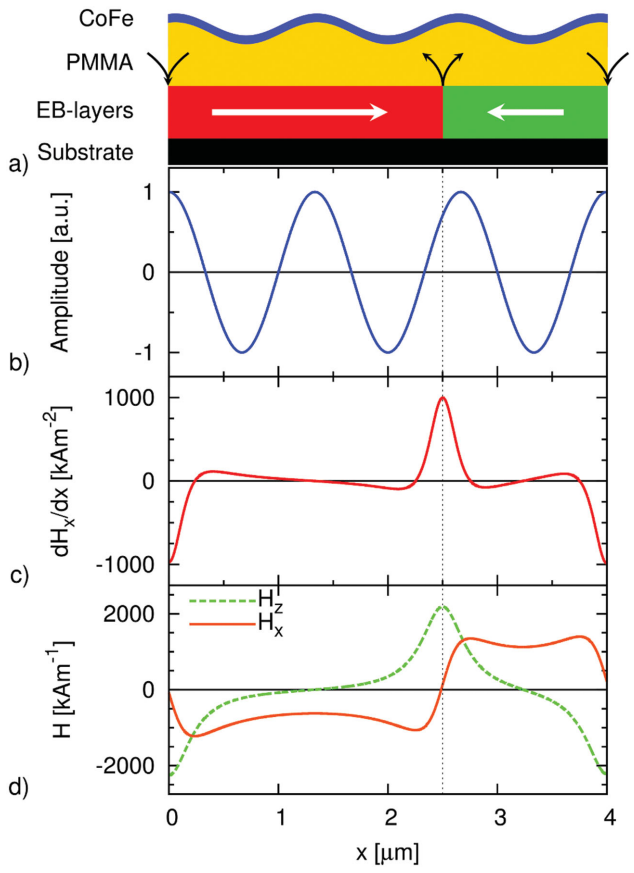

Figure 4. Interaction of magnetic stray fields and the topographic modulation due to wrinkling. In a) a schematic overview about the layer structure with the magnetic domains (red and green sections, magnetization directions are indicated by white arrows), the emerging stray fields (black arrows), and the wrinkling pattern is displayed as a cross-section. The following images give a detailed and separate look on those aspects with the fixed phase relation observed in our experiments. Panel b) depicts the idealized topographic modulation of the wrinkles with an arbitrary amplitude, c) is the gradient 100 nm above the surface of the ferromagnetic layer in the exchange bias system of the in-plane component H_x of the magnetic stray field which interacts with the ferromagnetic cap. d) The gradient is derived from the stray fields, which are calculated by numerical simulations and scaled to experimental data from micro-Hall measurements. c) The gradient exhibits three minima and three maxima per period of magnetic patterning which lead to additional strain in the ferromagnetic capping layer evoking the topographic deformation. For all graphs the lateral scale is identical and the dashed line at $x = 2.55$ µm together with the boundaries of the graph allow a correlation of the lateral position of the magnetic domain pattern, the emerging stray fields, and the topographic modulation of the wrinkles as described in the main text. The depicted lateral dimension of 4 µm represents a single period of magnetic domain pattern.

energy of layer deformation. Taking into account the rather narrow full width at half maximum of these peaks of about 250–600 nm, we conclude that the alignment of the initially randomly oriented wrinkles takes place when the commensurability of the period of the magnetic pattern and the wrinkled topography is achieved during the heating of the sample.

Based on this conclusion, we can readily explain the appearance of the two orthogonally oriented areas of aligned wrinkles (Figure 2a). When the transformation of the isotropic wrinkle pattern into the anisotropic one takes place, where wrinkles are aligned parallel to the magnetic domain walls, the strain in the isotropic system relaxes specifically anisotropic in the direction of the wrinkle wave vector.[7] The surrounding area must compensate for the not yet relaxed strain component in direction of the wrinkles, resulting in the wrinkles oriented essentially perpendicular to the underlying magnetic pattern.

4. Conclusion

We demonstrate the possibility to influence the morphology of self-organized wrinkling patterns in heterostructures consisting of a viscoelastic PMMA layer and a stiff magnetic layer by exposing it to periodic magnetic stray fields of artificially designed magnetic domains. Emerging stray fields from the parallel-stripe magnetic domain pattern of the substrate modify the wrinkling such that parallel wrinkles are formed, when the periodicity of the magnetic domain pattern is commensurate. In contrast, reference samples show random wrinkling, if no commensurate magnetic domain pattern is present.

The possibility to stabilize two distinct types of wrinkling patterns, namely, random and aligned, in the same material system opens up the possibility to develop a mechanically reconfigurable system: in the presented magnetically patterned layer system, aligned wrinkling will take place when commensurability to the underlying magnetic domain pattern is achieved. But if an in-plane magnetic field, strong enough to saturate the magnetic pattern, is applied during thermal annealing, the stray field influencing the wrinkling process will vanish leading to random wrinkling. As the wavelength and amplitude of the resulting surface structure can easily be adapted, i.e., by the lithography process in the case of the magnetic patterning and by the layer thickness in case of the wrinkle wavelength, a flexible and versatile platform for reconfigurable structures between random and aligned wrinkling is in prospect. The possibility to reconfigure the wrinkling pattern from being random to aligned by using external stimuli, e.g., magnetic fields, enables promising possibilities for stretchable electronics, such as magnetic field sensors[37,38] and tunable gratings for optoelectronics and photonics.[39]

5. Experimental Section

For the fabrication of the artificial magnetic field landscapes with parallel stripes, naturally oxidized silicon substrates were covered with an EB layer system ($Cu^{50\ nm}/Ir_{17}Mn_{83}^{10\ nm}/Co_{70}Fe_{30}^{6.5\ nm}/Ta^{10\ nm}$) deposited by radio frequency (RF) sputtering. The unidirectional anisotropy between the ferromagnetic and antiferromagnetic layer was initialized by field cooling at 300 °C in an in-plane external magnetic field of $H_{FC} = 70$ kA m^{-1}. The samples were characterized by vibrating sample magnetometry (VSM), showing a hysteresis loop with an exchange bias field of $H_{EB} = (-21.4 \pm 0.2)$ kA m^{-1} and a coercive field of $H_C = (4.6 \pm 0.2)$ kA m^{-1} (Figure 5a). These EB layer systems were magnetically patterned into parallel stripes with head-to-head and tail-to-tail magnetization orientations in adjacent domains with the magnetization vectors being oriented perpendicular to the domain walls by IBMP.[28–30] For this procedure photoresist masks of covered and uncovered stripes with a thickness of 750 nm were fabricated by UV-photolithography, where the stripes' long axes were aligned perpendicularly to the direction of

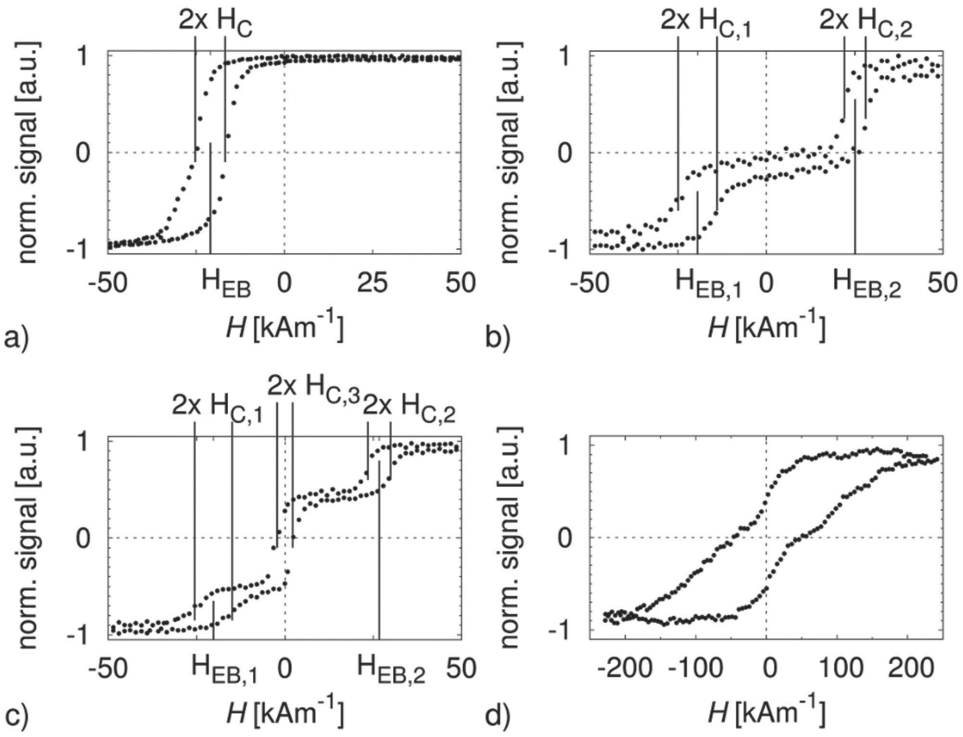

Figure 5. Hysteresis loops of the EB system after different steps of preparation, measured via vibrating sample magnetometry at room temperature: a) after field-cooling in order to initialize the exchange coupling, b) after ion bombardment induced magnetic patterning leading to two different types of magnetic domains with opposite in-plane magnetization, and c) after the deposition of the additional cap on top of the PMMA with the characteristics of an uncoupled ferromagnetic film. Panel d) shows the out-of-plane hysteresis of a single 9 nm CoFe film fabricated by sputter deposition. The characteristic values of coercive and EB field for the (partial) hysteresis loops are indicated in a), b), and c), numbers are listed within the main text.

the unidirectional magnetic anisotropy. Samples with stripe widths of about $W \approx 2$, 5, and 10 µm were fabricated. The deposited film systems with resist masks were then bombarded with 10 keV He^+ ions from a home-built plasma ion source[40] with a fluency of 2×10^{15} cm^{-2} in an external magnetic field of $H_{IB} = 80$ kA m^{-1} oriented antiparallel to the direction of the initialized unidirectional magnetic anisotropy.[31,41] After ion bombardment, the resist has been removed by an aqueous solution of potassium hydroxide (3%) and subsequently by pure acetone using an ultrasonic bath. After resist removal, the samples were again characterized by VSM, showing the bipartite hysteresis loop of Figure 5b, corresponding to the two oppositely exchange biased artificial domains. The two EB and coercive fields of the two hysteresis loop parts were $H_{EB,1} = (-19.3 \pm 0.6)$ kA m^{-1}, $H_{C,1} = (5.3 \pm 0.3)$ kA m^{-1}, $H_{EB,2} = (25.1 \pm 0.5)$ kA m^{-1}, $H_{C,2} = (3.0 \pm 0.2)$ kA m^{-1}. Additional measurements by AFM/MFM were performed showing parallel stripe domains with antiparallel magnetizations perpendicular to the long stripe axis in adjacent domains. The magnetization configuration in these artificial domains induces charged domain walls with maximum stray field emission over the walls, generating a periodic magnetic stray field landscape.[32] In the next step of preparation, a thin film of polymethylmethacrylate (Sigma-Aldrich Co., $M_W = 120\,000$ g mol^{-1}, $T_g = 114$ °C)[36] was deposited on top of the Ta layer by spin coating at 4000 rpm (64 s, including linear acceleration and deceleration for 2 s each) of a solution with 3-pentanone ($c = 25$ mg mL^{-1}). The resulting layer thickness was determined by variable angle ellipsometry to be in the range of 90–95 nm for individual samples. The last step of sample fabrication was the deposition of the ferromagnetic capping layer ($Co_{70}Fe_{30}$) with a thickness of 9 nm by RF-sputter deposition. The thickness of this CoFe layer has been chosen to display strong easy-plane anisotropy. A further VSM characterization of the complete layer system prior to heating (Figure 5c) showed three loops, the outer ones corresponding to the patterned EB system and the inner loop corresponding to the ferromagnetic capping layer. The determined EB- and coercive fields were $H_{EB,1} = (-20.2 \pm 0.7)$ kA m^{-1}, $H_{C,1} = (5.3 \pm 0.4)$ kA m^{-1}, $H_{EB,2} = (26.7 \pm 0.3)$ kA m^{-1}, $H_{C,2} = (3.2 \pm 0.2)$ kA m^{-1}, $H_{C,3} = (2.2 \pm 0.2)$ kA m^{-1}. EB and coercive fields of the patterned EB layer system have almost not changed during the procedure.

To initialize wrinkling, the samples were annealed on a hotplate where they were heated to 150 °C from room temperature at a rate of 32.5 °C min^{-1}. After 1 min at 150 °C the samples were cooled down to room temperature quickly by removing them from the hotplate. The wrinkling occurred during the heating step and was visible by the bare eye (also Figure 3b). The mechanical properties of the PMMA and CoFe layer lead to the conclusion that wrinkling was driven by a compressive stress on the cap layer.[42] The annealing temperature has been chosen to be below the blocking temperature of the EB layer system. The resulting wrinkling patterns were characterized by AFM using a 2D autocorrelation function for the determination of the wavelength of wrinkling with a typical uncertainty of about $\Delta W_w = 100$ nm.

Supporting Information

Supporting Information is available from the Wiley Online Library or from the author.

Acknowledgements

M.M. and D.M. acknowledge the partial financing of this work via the European Research Council within the European Union's Seventh

Framework Programme (FP7/2007–2013)/ERC grant agreement no. 306277.

Received: July 29, 2015
Revised: September 7, 2015
Published online: October 7, 2015

[1] J. Chen, N. C. Seeman, *Nature* **1991**, *350*, 631.
[2] A. Bétard, R. A. Fischer, *Chem. Rev.* **2012**, *112*, 1050.
[3] J.-H. Cho, D. H. Gracias, *Nano Lett.* **2009**, *9*, 4049.
[4] P. J. Yoo, K. Y. Suh, S. Y. Park, H. H. Lee, *Adv. Mater.* **2002**, *14*, 1383.
[5] M. Müller-Wiegand, G. Georgiev, E. Oesterschulze, T. Fuhrmann-Lieker, J. Salbeck, *Appl. Phys. Lett.* **2002**, *81*, 4940.
[6] D. Breid, A. J. Crosby, *Soft Matter* **2011**, *7*, 4490.
[7] N. Bowden, S. Brittain, A. G. Evans, J. W. Hutchinson, G. M. Whitesides, *Nature* **1998**, *393*, 146.
[8] X. Chen, J. W. Hutchinson, *J. Appl. Mech.* **2004**, *71*, 597.
[9] C. M. Stafford, C. Harrison, K. L. Beers, A. Karim, E. J. Amis, M. R. VanLandingham, H.-C. Kim, W. Volksen, R. D. Miller, E. E. Simonyi, *Nat. Mater.* **2004**, *3*, 545.
[10] E. P. Chan, S. Kundu, Q. Lin, C. M. Stafford, *ACS Appl. Mater. Interfaces* **2011**, *3*, 331.
[11] S. Kundu, C. S. Davis, T. Long, R. Sharma, A. J. Crosby, *J. Polym. Sci., Part B: Polym. Phys.* **2011**, *49*, 179.
[12] J. A. Rogers, T. Someya, Y. Huang, *Science* **2010**, *327*, 1603.
[13] S. Wagner, S. Bauer, *MRS Bull.* **2012**, *37*, 207.
[14] J. A. Rogers, M. G. Lagally, R. G. Nuzzo, *Nature* **2011**, *477*, 45.
[15] X. Wang, H. Hu, Y. Shen, X. Zhou, Z. Zheng, *Adv. Mater.* **2011**, *23*, 3090.
[16] J. Jones, S. P. Lacour, S. Wagner, S. B. Z. Suo, *J. Vac. Sci. Technol., A* **2004**, *22*, 1723.
[17] M. Drack, I. Graz, T. Sekitani, T. Someya, M. Kaltenbrunner, S. Bauer, *Adv. Mater.* **2015**, *27*, 34.
[18] M. Melzer, D. Makarov, A. Calvimontes, D. Karnaushenko, S. Baunack, R. Kaltofen, Y. Mei, O. G. Schmidt, *Nano Lett.* **2011**, *11*, 2522.
[19] M. Melzer, M. Kaltenbrunner, D. Makarov, D. Karnaushenko, D. Karnaushenko, T. Sekitani, T. Someya, O. G. Schmidt, *Nat. Commun.* **2015**, *6*, 6080.
[20] M. Melzer, D. Karaushenko, G. Lin, S. Baunack, D. Makarov, O. G. Schmidt, *Adv. Mater.* **2015**, *27*, 1333.
[21] D.-H. Kim, J.-H. Ahn, W. M. Choi, H. S. Kim, J. Song, Y. Y. Huang, Z. Liu, C. Lu, J. A. Rogers, *Science* **2008**, *320*, 507.
[22] J. Genzer, J. Groenewold, *Soft Matter* **2006**, *2*, 310.
[23] Z. Shen, L. Wu, S. Zhu, Y. Zheng, X. Chen, *Appl. Phys. Lett.* **2014**, *105*, 021106.
[24] T. R. Hendricks, W. Wang, I. Lee, *Soft Matter* **2010**, *6*, 3701.
[25] N. Bowden, W. T. S. Huck, K. E. Paul, G. M. Whitesides, *Appl. Phys. Lett.* **1999**, *75*, 2557.
[26] C.-M. Chen, J. C. Reed, S. Yang, *Soft Matter* **2013**, *9*, 11007.
[27] H. Vandeparre, J. Léopoldès, C. Poulard, S. Desprez, G. Derue, C. Gay, P. Damman, *Phys. Rev. Lett.* **2007**, *99*, 188302.
[28] A. Mougin, S. Poppe, J. Fassbender, B. Hillebrands, G. Faini, U. Ebels, M. Jung, D. Engel, A. Ehresmann, H. Schmoranzer, *J. Appl. Phys.* **2001**, *89*, 6606.
[29] J. Fassbender, S. Poppe, T. Mewes, A. Mougin, B. Hillebrands, D. Engel, M. Jung, A. Ehresmann, H. Schmoranzer, G. Faini, K. J. Kirk, J. N. Chapman, *Phys. Status Solidi A* **2002**, *189*, 439.
[30] A. Ehresmann, I. Krug, A. Kronenberger, A. Ehlers, D. Engel, *J. Magn. Magn. Mater.* **2004**, *280*, 369.
[31] A. Ehresmann, D. Engel, T. Weis, A. Schindler, D. Junk, J. Schmalhorst, V. Höink, M. D. Sacher, G. Reiss, *Phys. Status Solidi B* **2006**, *243*, 29.
[32] D. Holzinger, N. Zingsem, I. Koch, A. Gaul, M. Fohler, C. Schmidt, A. Ehresmann, *J. Appl. Phys.* **2013**, *114*, 013908.
[33] F. Ahrend, D. Holzinger, M. Fohler, S. Pofahl, U. Wolff, M. DeKieviet, R. Schaefer, A. Ehresmann, *J. Magn. Magn. Mater.* **2015**, *381*, 292.
[34] A. Ehresmann, D. Lengemann, T. Weis, A. Albrecht, J. Langfahl-Kalbes, F. Göllner, D. Engel, *Adv. Mater.* **2011**, *23*, 5568.
[35] R. Huang, S. H. Im, *Phys. Rev. E: Stat.* **2006**, *74*, 026214.
[36] T_g was determined by differential scanning calorimetry (DSC) prior to the preparation of the solution for spin-coating.
[37] M. Melzer, G. Lin, D. Makarov, O. G. Schmidt, *Adv. Mater.* **2012**, *24*, 6468.
[38] M. Melzer, D. Karnausshenko, D. Makarov, L. Baraban, A. Calvimontes, I. Mönch, R. Kaltofen, Y. Mei, O. G. Schmidt, *RSC Adv.* **2012**, *2*, 2284.
[39] T.-K. Shih, J.-R. Ho, H.-Y. Liao, C.-F. Chen, C.-Y. Liu, *Thin Solid Films* **2008**, *516*, 5339.
[40] D. Lengemann, D. Engel, A. Ehresmann, *Rev. Sci. Instrum.* **2012**, *83*, 053303.
[41] J. McCord, R. Schäfer, K. Theis-Bröhl, H. Zabel, J. Schmalhorst, V. Höink, H. Brückl, T. Weis, D. Engel, A. Ehresmann, *J. Appl. Phys.* **2005**, *97*, 10K102.
[42] W. Martienssen, H. Warlimont, *Springer Handbook of Condensed Matter and Materials Data*, Springer-Verlag, Berlin, Germany **2005**, p. 132, 498.